SANDIA REPORT

OFFICIAL USE ONLY

SAND88—3046
Printed March 1989

Enclosure 1: #60

Force Reconstruction for the G-M118 Field Test of the Strategic Earth Penetrator Weapon (SEPW)

Vesta I. Bateman

Prepared by
Sandia National Laboratories
Albuquerque, New Mexico 87185 and Livermore, California 94550
for the United States Department of Energy
under Contract DE-AC04-76DP00789

OFFICIAL USE ONLY

Contains information which may be exempt from public release under the Freedom of Information Act (5 USC 552), exemption number(s) 5. Approval by the Department of Energy prior to public release is required.

Originator: T. G. Priddy Date: March 3, 1989

CONFIRMED TO BE UNCLASSIFIED
AUTHORITY DOE/NN-52
BY R.H. SMILEY RHS, ADD,
2-22-96
Nancy Connelly, ADD, 5010.23, 7/8/05
HR Schmidt, HS-93, 5/11/07

OFFICIAL USE ONLY

SF2900Q(8-81)

8783

955A20B000277

SAND88-3046
OFFICAL USE ONLY
Printed March 1989

FORCE RECONSTRUCTION FOR THE G-M118 FIELD TEST OF THE STRATEGIC EARTH PENETRATOR WEAPON (SEPW)

Vesta I. Bateman
Experimental Mechanics Department
Sandia National Laboratories

ABSTRACT

A field test at Tonopah Test Range was conducted to demonstrate a force reconstruction technique for the Strategic Earth Penetrator Weapon (SEPW). The penetrator was instrumented with four strain gages at the same axial location on the penetrator case interior and with one axial accelerometer in the data acquisition system. A deconvolution technique was employed to reconstruct three orthogonal forces (one axial and two lateral) from the strain gage data and an axial force from the accelerometer data. The two axial forces are compared and discussed. The two lateral forces are the first lateral forces reconstructed from penetrator data at Sandia.

OFFICAL USE ONLY

Contains information which may be exempt from public release under the Freedom of Information Act (5 USC 552), exemption number 5. Approval by the Department of Energy prior to public release is required.

Originator: Thomas G. Priddy Date: 03-03-89

ACKNOWLEDGEMENTS

The author thanks the following people whose efforts allowed this work: Larry R. Dorrell, 7542, for strain gage installation; James P. Lauffer, 7543, and Fred A. Brown, 7541, for acquiring the structural data; Ned R. Hansen, 5165, for conducting the field test; Otis M. Solomon, Jr. and Gene C. Hauser, 5144, for acquiring the field data; Robert J. Kipp, 1522, for providing analyses of the SEPW structure and of the predicted penetration environment; and David O. Smallwood, 7544, and Ned R. Hansen, 5165, for their thoughtful review of this report.

CONTENTS

INTRODUCTION
STRUCTURAL CHARACTERIZATION TESTS
STRUCTURAL FREQUENCY RESPONSE FUNCTIONS
FORCE RECONSTRUCTION WITH A DECONVOLUTION TECHNIQUE
DISCUSSION AND CONCLUSIONS
REFERENCES

FIGURES

1 Reverse Hopkinson Bar Test Configuration
2 Reverse Hopkinson Bar Axial Input Forces
3 SEPW Strain Responses to Reverse Hopkinson Bar Axial Force Input
4 SEPW Axial Acceleration Frequency Response Function
5 SEPW Strain Frequency Response Functions for Axial Input Force
6 SEPW Strain Frequency Response Functions for Lateral (02) Input
7 SEPW Strain Frequency Response Functions for Lateral (13) Input
8 The Inverse of the Axial Frequency Response Function for An Axial Input Force (h_{11}^{-1})
9 The Inverse of the Lateral Frequency Response Function (02 plane) for an Axial Force Input (h_{12}^{-1})
10 G-M118 Measured Axial Acceleration
11 G-M118 Axial Force Reconstructed from Axial Acceleration
12 G-M118 Axial Strain Response
13 G-M118 Axial Force Reconstructed from Three Orthogonal Strain Strain Responses
14 G-M118 Lateral (02 plane) Strain Response
15 G-M118 Lateral (02 plane) Force Reconstructed from Three Orthogonal Strain Responses
16 G-M118 Lateral (13 plane) Strain Response
17 G-M118 Lateral (13 plane) Force Reconstructed from Three Orthogonal Strain Responses
18 Comparison of Axial Strain Response and Reconstructed Axial Force for G-M118
19 Comparison of with Axial Force Reconstructed by Deconvolution and Axial Force from Filtered Acceleration Data
20 Comparison of Predicted Force Using GNOME with Reconstructed Forces by Deconvolution from Acceleration and Strain Data
21 G-M118 Predicted Lateral Forces at the Nose and Tail Using GNOME

FORCE RECONSTRUCTION FOR THE G-M118 FIELD TEST OF THE STRATEGIC EARTH PENETRATOR WEAPON (SEPW)

INTRODUCTION

The force environment experienced during earth penetration is important to earth penetrator development because it determines the warhead survival criteria for both the penetrator case and the internal components. This report presents a deconvolution technique for reconstructing penetration forces from field test data. The force reconstruction was undertaken to provide a better estimate of the forces and to verify the analytical prediction of the penetration forces.

In the past, axial forces have been estimated from acceleration data by digitally filtering the data to a frequency below which the structure is assumed to act like a rigid body; the resulting acceleration is multiplied by the mass of the structure to obtain the axial force. The frequency content in this force is restricted to the cut-off frequency of the digital filter, and the rise-time of the force can be no faster than that of the filter. The deconvolution technique can potentially provide greater frequency content in the force and preserve the rise-time of the initial force peak. However, the deconvolution technique requires both high quality estimates of the penetrator's structural characteristics and high quality penetration data. Estimates of structural characteristics are obtained with laboratory tests.

The penetration data was obtained in a field test of the scale model for the Strategic Earth Penetrator Weapon (SEPW), G-M118, that was conducted for the purpose of force reconstruction at Tonopah Test Range. The SEPW was fired from the Davis Gun at a 60 degree impact angle and 0 degree angle of attack with a measured velocity of 1940 fps into Antelope Tuff. The surveyed path length of the penetration was 14.6 ft. The penetrator was instrumented with an axial accelerometer located in the data acquisition system (about 16.5 inches from the penetrator nose tip) and four strain gages located on the case interior and installed 90 degrees apart along the circumference at an axial location of 23.1 inches from the penetrator nose tip. Details of the penetrator test hardware are documented in Sandia Drawing S78589. The response data were recorded with an eight-bit, battery operated data acquisition system mounted in the SEPW; each strain and acceleration channel in this system had a frequency response from 0 Hz through 9600 Hz [1].

the solution of (3) implicitly assumes that the penetration forces act as point forces on the SEPW nose.

Although the solution to (3) appears straightforward, there are problems which arise in its solution. Noise, either electrical or structural (variations in response which do not fit the linear model), can be amplified in the solution, so the effects of noise must be diminished in some manner. The inversion of the $\underline{H}$ matrix exacerbates this problem since small values are amplified in the inversion process. Additionally, structural coupling and the existence of structural node points may cause ill-conditioning of $\underline{H}^{-1}$. The problems which arose in the analysis of the G-M118 data are discussed below.

STRUCTURAL CHARACTERIZATION TESTS

The configuration of the SEPW for the structural tests is the same as that for the field test. The SEPW case is 41.2 in long, and the outside cylindrical diameter is 8.245 in. The unit weighs 376 lbs: the case weighs 186 lbs and the internal components weigh 190 lbs. About 100 lbs of the internal components are held in place by a threaded ring; the remaining 90 lbs are installed aft and followed by another ring. The data acquisition system is included in the forward 100 lbs.

A high-level force input was applied to the SEPW structure in order to measure quantities necessary for calculation of the frequency response functions. The force was generated using the Reverse Hopkinson Bar technique developed at Sandia Laboratories where a bar is propelled by an air gun towards the test object as shown in Figure 1. In this configuration, the bar provides a force input to the structure whose

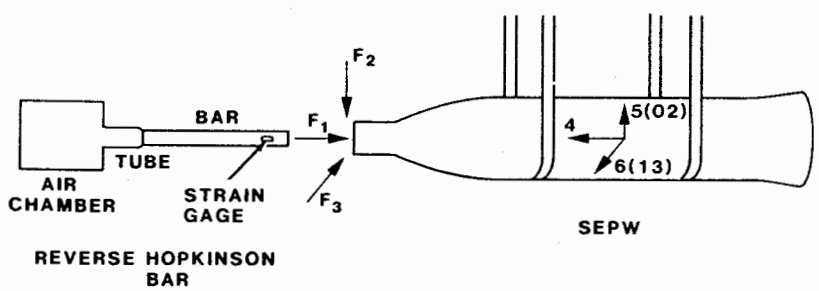

FIGURE 1: Reverse Hopkinson Bar Test Configuration

characteristics are governed by one-dimensional wave theory with the duration of the force controlled by the length of the bar [2]. A 1-inch diameter and 10-inch long bar was used for these structural measurements. The force generated in the bar during impact is measured with strain gages mounted 2 inches from the impact end. The strain gages measure the correct amplitude of the force pulse, but the duration of the pulse must be corrected for the measurement location. This technique generates a high-level force with a duration of about 100 μs when it impacts the SEPW. The short duration of the force pulse excites structural frequencies up to 10 kHz [3] and was used because the structural characteristics were desired up to the 9600 Hz frequency available in the penetration data [1]. The SEPW was mounted in a free-free boundary condition, and the high-level force was

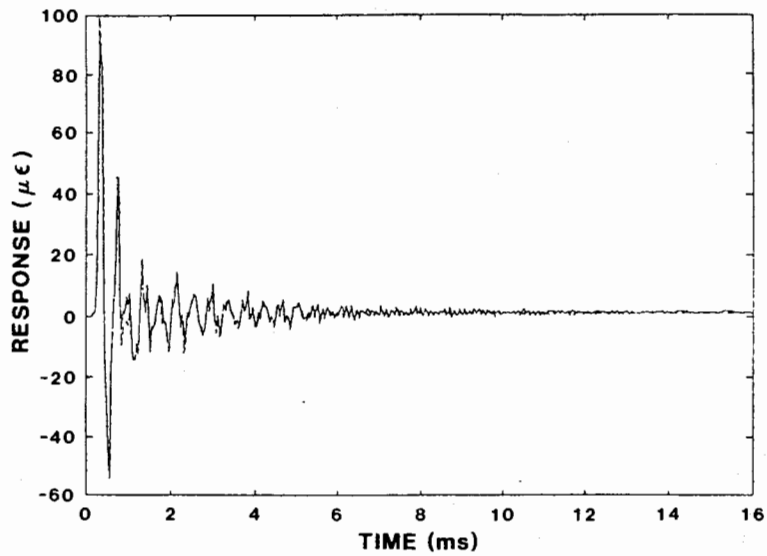

FIGURE 3: SEPW Strain Responses to Reverse Hopkinson Bar Axial Force Input

If the force is estimated simply by digitally filtering the acceleration penetration data, the modal frequencies provide an upper limit for the force estimate and indicate that the data should be filtered below 1800 Hz for axial data and 942 Hz for lateral data. These modal frequencies provide a lower bound for the deconvolution force reconstruction. Since the purpose of the deconvolution technique is to reconstruct the excitation forces based on structural response data that may reflect elastic vibration of the structure, the force reconstruction should extend beyond the lowest modal frequencies of 1800 Hz for axial and 942 Hz for lateral forces.

STRUCTURAL FREQUENCY RESPONSE FUNCTIONS

The structural frequency response functions which comprise the nine elements of the $\underline{H}$ matrix were calculated from the measurements described above with the equation

$$H_{ki} = \frac{G_{fr}}{G_{ff}} \tag{4}$$

where G_{fr} is the cross-spectrum between the force and the appropriate response and G_{ff} is the auto-spectrum for the force input. In (4), the subscript k represents the direction of the force input, and the subscript i represents the corresponding response in accordance with the directions shown in Figure 1. This formula for the frequency response function was used because it provides an accurate estimate when there is noise in the response [5] which is the case for structural measurements. The noise in the response may be either electrical or structural; both types were evident in the response measurements for the SEPW.

The first step in the calculation of the frequency response functions was to account for a difference in sample rates between the data from the structural tests and the penetration data from the field test. Because of a catastrophic failure of the batteries in the original data acquisition system after the structural tests [6], another data acquisition system was constructed and fielded. The sample rates and cut-off frequencies for the analog filters were different for the two systems, but all other characteristics were the same. The first system had a sample rate of 24,255 Hz and a cut-off frequency of 4800 Hz; the second system had a sample rate of 34,426 Hz and a cut-off frequency of 9600 Hz. Both systems had a cascade of two, 2-pole Butterworth lowpass analog filters to prevent aliasing. The sample rate of the structural test data with the first system was interpolated by a factor of 10 and then decimated by 7 so that the resulting sample rate was 34,650 Hz which differs from 34,426 Hz by less that 1%. The sample rate for the laboratory force measurement was 2 MHz; the force data were digitally filtered by a 4-pole Butterworth filter with a cut-off frequency of 4800 Hz and then decimated by 58. The resulting sample rates for the force and response measurements for the structural tests differed by less than 0.5%.

For the frequency response function calculations as well as for all calculations in the force estimation process, a vector of 8192 points was used for each quantity. These vectors were formed by adding zeros to the data and were used to improve frequency resolution [7]; a resolution of 4.2 Hz in the frequency domain resulted. The cross-spectrum and auto-spectrum functions were formed from the response and force measurements with the additional zeros. The functions were averaged for five impacts with the Reverse Hopkinson bar in the axial direction and for three impacts with the Reverse Hopkinson bar in each of the two lateral directions. The functions exhibited considerable

noise at low frequencies which was observed in both the magnitude and phase of the frequency response function. Since this noise appeared at frequencies below 500 Hz, it could not represent structural resonances; it appeared to be electrical noise which must be eliminated to prevent ill-conditioning in $\underline{H}^{-1}$. The noise was eliminated by fitting the strain low frequency asymptote in the frequency domain with the function

$$H(j\omega) = ae^{\alpha\omega} + j\phi ae^{\alpha\omega} \tag{5}$$

where a is a constant chosen as described below, α was chosen to fit the data, ω is circular frequency in rad/sec, ϕ is the phase of $H(j\omega)$ in rad, and j is the square root of -1. The magnitude and phase in (5) are smooth functions which approximate the strain response of a second-order mechanical system at low frequencies which could not be measured accurately in the presence of electrical noise [8]. The acceleration low frequency asymptote was fit by a similar technique which has been derived for acceleration data [9]. The asymptotic fit of the frequency response functions with these functions has a smoothing effect on both the phase and the magnitude. This smoothing in the frequency-domain is equivalent to decreasing the duration of the impulse response function in the time-domain [10] because if

$$H(j\omega) = A \cdot \exp(j\phi) \tag{6}$$

where A is the magnitude of $H(j\omega)$, then,

$$\int_{-\infty}^{\infty} t^2 h^2(t)dt = \int_{-\infty}^{\infty} \left[\left(\frac{dA}{d\omega}\right)^2 + \omega^2 \left(\frac{d\phi}{d\omega}\right)^2 \right] d\omega \tag{7}$$

where t is time and h(t) is the impulse response function that corresponds to $H(j\omega)$. This property is useful in the deconvolution process because the impulse response function, and consequently its inverse, will have a shorter duration in the time domain as a result of the smoothing process.

The low frequency asymptote magnitude values for the SEPW frequency response functions determine the magnitude of the reconstructed forces and were calculated with a Shell Shock Structural Code [11] model of the SEPW by Robert J. Kipp, Division 1522, because these measurements could not be made in the laboratory. The magnitudes correspond to a constant acceleration at zero frequency and should be non-zero for the response in the same axis as the force input. Out-of-axis response should be very low if the input force is correctly aligned with the structure, and a non-zero magnitude represents noise. The in-axis frequency response function asymptote values are

$$H_{11}(0) = 5.3 \times 10^{-4}\ \mu\varepsilon/\text{lb} \tag{8}$$

and

$$H_{22}(0) = H_{33}(0) = 4.3 \times 10^{-3}\ \mu\varepsilon/\text{lb} \tag{9}$$

Since the SEPW is essentially axisymmetric about the axial direction, the values for $H_{22}(0)$ and $H_{33}(0)$ are the same because $I_{22} \approx I_{33}$.

The values for the constant, a, in (5) are in (8) and (9) for the in-axis strain frequency response functions. In the absence of other information, the magnitudes of the asymptotes for the out-of-axis strain frequency response functions were set to $10^{-5}\ \mu\varepsilon/\text{lb}$ which is more than an order of magnitude lower than the in-axis values. The low frequency asymptote for the acceleration frequency response function is the inverse of the weight [9] or 2.7×10^{-3} g/lb. The acceleration frequency response function is shown in Figure 4, and the strain frequency response functions are shown in Figures 5-7. For the strain frequency response functions, one column of the frequency response function matrix, $\underline{H}$, is depicted in each figure where one frequency response function represents response in the same axis as the applied force. The other two functions in the figure represent the out-of-axis response and may be due either to structural coupling or to excitation in the respective axis because the Reverse Hopkinson Bar was slightly misaligned. Since the out-of-axis response was very consistent, it is doubtful that it is due to misalignment of the Reverse Hopkinson Bar because misalignment errors are random. The frequency response functions were truncated at 3360 Hz for axial response and 1932 Hz for lateral response because of structural noise in the functions. This structural noise may be due to non-linearities in the SEPW structure.

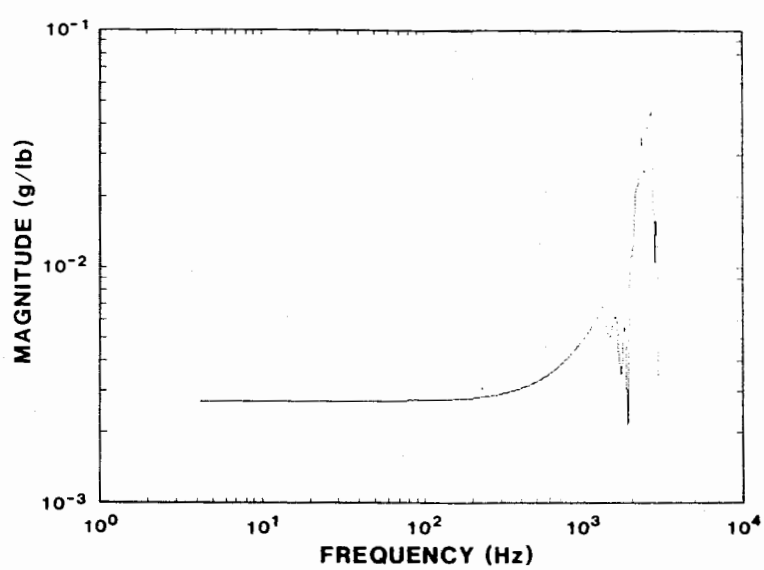

FIGURE 4: SEPW Axial Acceleration Frequency Response Function

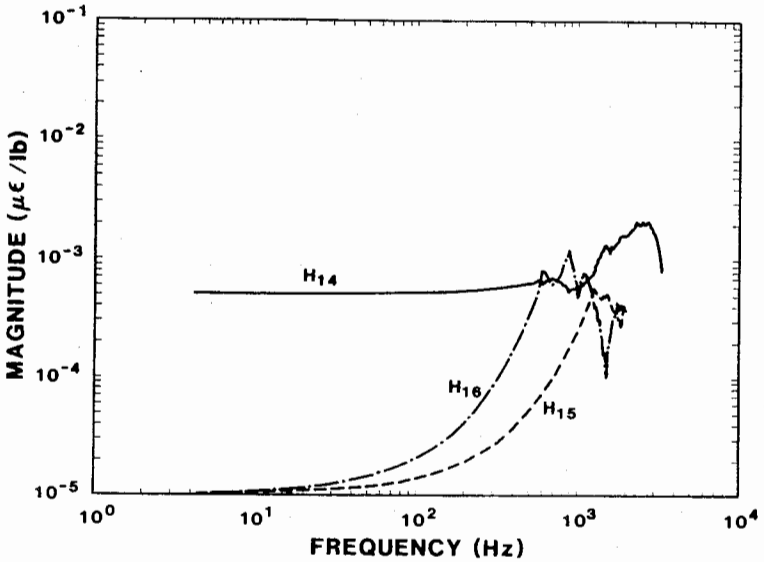

FIGURE 5: SEPW Strain Frequency Response Functions for Axial Input Force

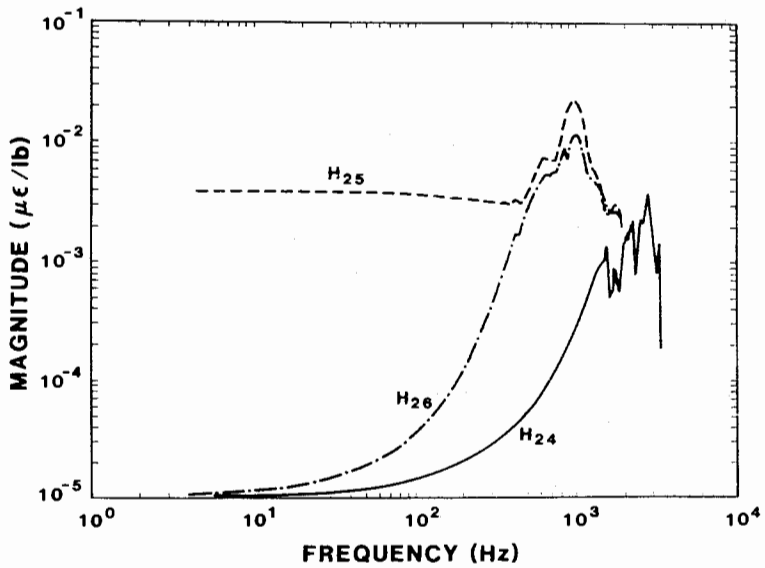

FIGURE 6: SEPW Strain Frequency Response Functions for Lateral (O2) Input

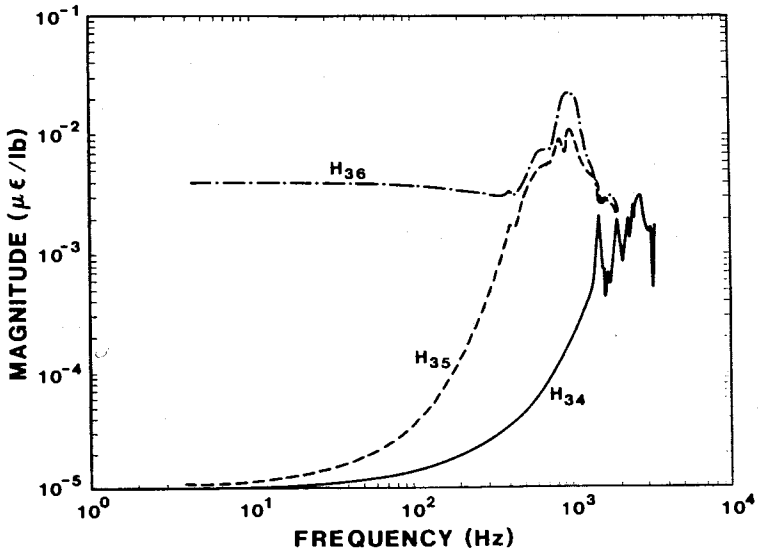

FIGURE 7: SEPW Strain Frequency Response Functions for Lateral (13) Input

FORCE RECONSTRUCTION WITH A DECONVOLUTION TECHNIQUE

In the deconvolution force reconstruction process, the inverse of the matrix of frequency response functions, $\underline{H}^{-1}$, is formed from

$$\underline{H}^{-1} = [[\underline{H}^*]^T \cdot \underline{H}]^{-1} \cdot [\underline{H}^*]^T \tag{10}$$

where $[\underline{H}^*]^T$ is the conjugate transpose of $\underline{H}$. In this formulation, $\underline{H}^{-1}$ is the pseudo-inverse and represents the equivalent of a least-squares solution to the force estimate in equation (3) [12]. The components of $\underline{H}^{-1}$ are, by definition, non-causal because of the delay in the response of the strain gages and accelerometer to the force input which becomes response in negative-time when $\underline{H}^{-1}$ is transformed into the time-domain as $\underline{h}^{-1}$ [13]. This non-causality is demonstrated in Figures 8 and 9. In Figure 8, the axial impulse response function for

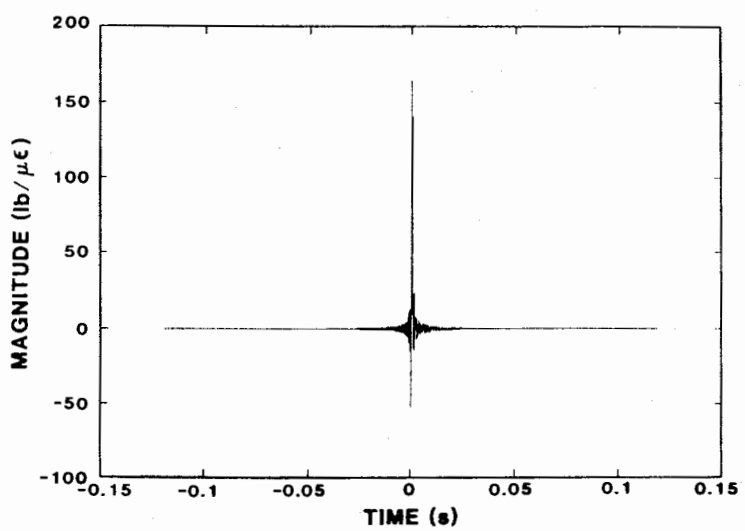

FIGURE 8: The Inverse of the Axial Frequency Response Function for an Axial Input Force (h_{11}^{-1})

an axial input, h_{11}^{-1}, is shown with both negative and positive time elements so that the envelope of the function can be seen. This impulse response is that for a physically non-realizable system as evidenced by the fact it has non-zero values for $t<0$. In Figure 9, another element of the $\underline{h}^{-1}$ matrix is shown. This element, h_{21}^{-1}, is the lateral (02 plane) response to the axial input force. As in Figure 8, the function's negative and positive time elements are plotted. There is a higher noise to signal ratio evident in h_{21}^{-1} as compared to h_{11}^{-1}, but its magnitude is considerably lower, which allows its use in the force reconstruction process. Figures 8-9 demonstrate the typical characteristics of the elements of the $\underline{h}^{-1}$ matrix; the other elements of $\underline{h}^{-1}$ are similar.

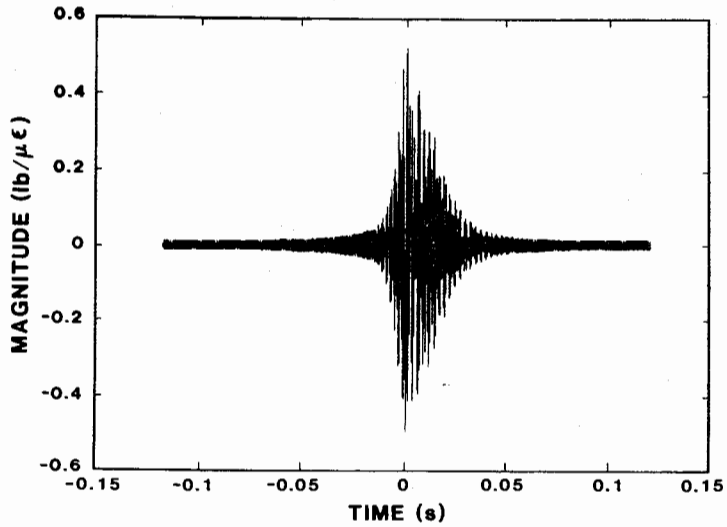

FIGURE 9: The Inverse of the Lateral Frequency Response Function (02 plane) for an Axial Force Input (h_{12}^{-1})

In accordance with equation (3), the inverse of the acceleration frequency response function in Figure 4 was combined with the measured acceleration from G-M118 to reconstruct the axial force from the acceleration data; the $\underline{H}^{-1}$ matrix was combined with the three orthogonal strain responses resolved from the G-M118 measured strain to reconstruct three forces from the strain data. For each response, only the portion of the record from impact to the end of the event was used; the record corresponded to about 20 ms or 675 data points in each case. At the end of the 675 response points, the penetration event is considered complete, and the SEPW has zero velocity. The responses were combined with a sufficient number of zeros to form vectors of 8192 points as discussed previously.

The measured axial acceleration from G-M118 is plotted in Figure 10; the axial force reconstructed from this acceleration with a one-dimensional deconvolution technique is in Figure 11. The three orthogonal strains resolved from the G-M118 strain data are each plotted and followed by their respective force reconstructed from a three-dimensional deconvolution technique: axial strain and reconstructed force are in Figures 12-13; lateral (02) strain and reconstructed force are in Figures 14-15; and lateral (13) strain and reconstructed force are in Figures 16-17.

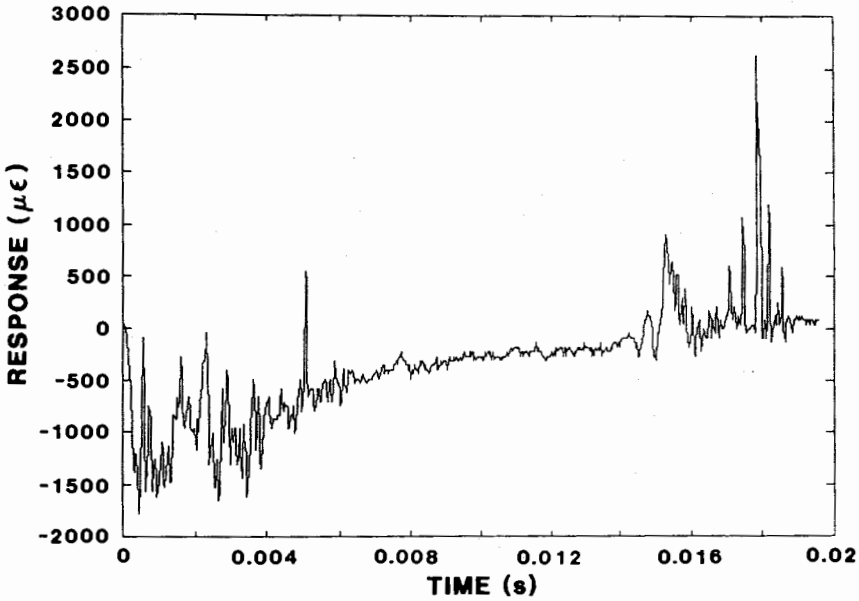

FIGURE 12: G-M118 Axial Strain Response

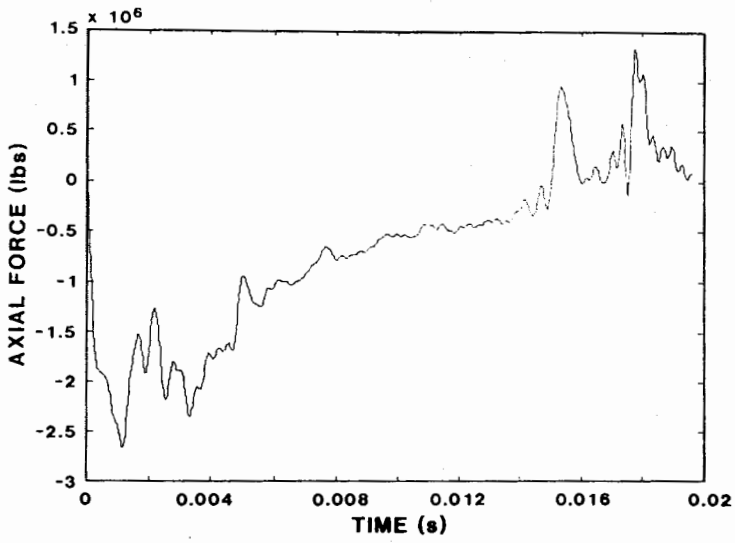

FIGURE 13: G-M118 Axial Force Reconstructed from Three Orthogonal Strain Responses

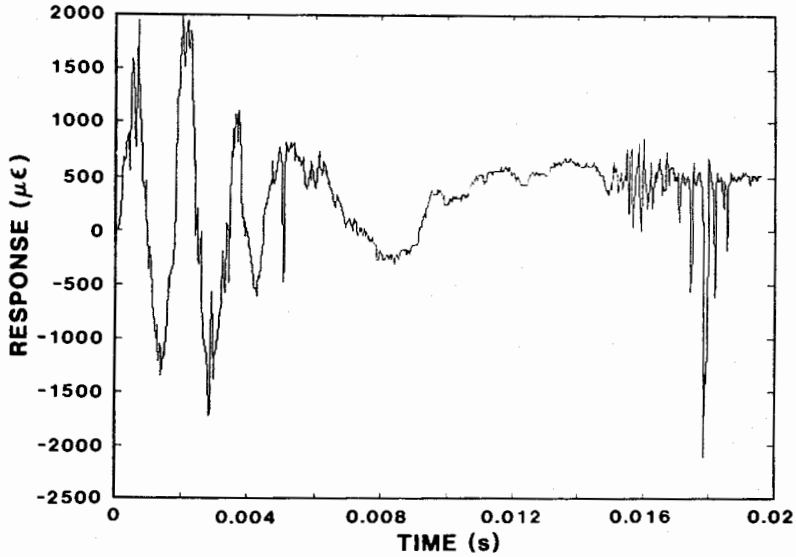

FIGURE 14: G-M118 Lateral (02 plane) Strain Response

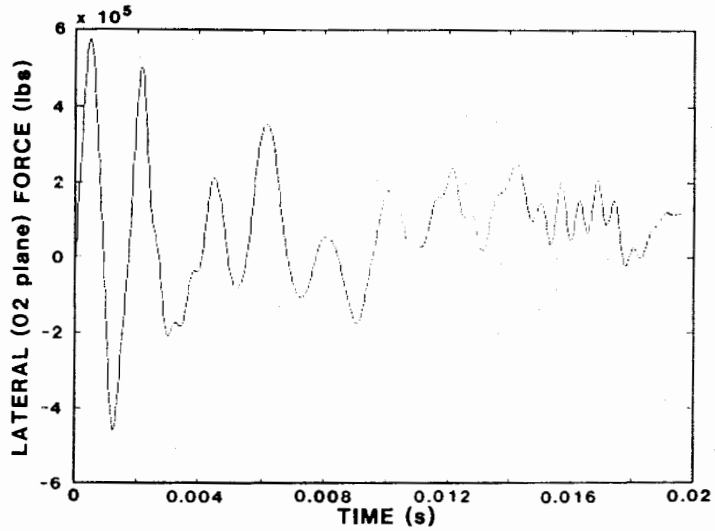

FIGURE 15: G-M118 Lateral (02 plane) Force Reconstructed from Three Orthogonal Strain Responses

DISCUSSION AND CONCLUSIONS

The results presented in this report are the reconstructed forces acting on the SEPW during the G-M118 field test. The forces include frequency content up to 3360 Hz for axial forces and 1932 Hz for lateral forces. The axial forces were reconstructed from both acceleration and strain responses; the lateral forces were reconstructed from strain responses. The two lateral forces are the first lateral forces reconstructed from penetrator data at Sandia. The deconvolution technique used for the reconstruction preserved the rise-time in the force by extending the frequency content over that possible by estimating the force from filtered data. This is demonstrated in Figure 18 where the axial strain is compared to

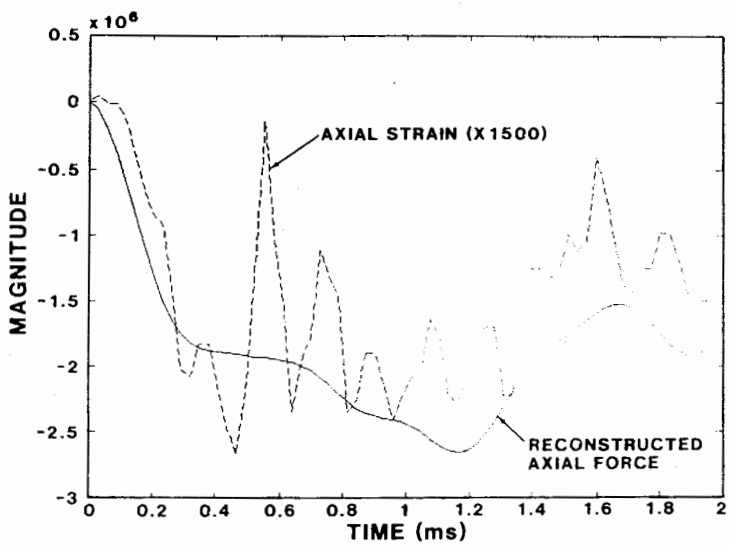

FIGURE 18: Comparison of Axial Strain and Reconstructed Axial Force for G-M118

the reconstructed force for the initial 2 ms of the penetration event. Additionally, a comparison of any strain or acceleration response with its corresponding force in Figures 10-17 shows that the force cannot be inferred from the response.

An axial force was computed with filtered acceleration data. The axial acceleration data was filtered by a 4-pole Butterworth filter with a cut-off frequency of 1000 Hz; the resulting acceleration data was multiplied by the SEPW weight to obtain the axial force. The 1000 Hz cut-off frequency was chosen because it is about one-half of the lowest axial frequency for the SEPW which is 1800 Hz. The axial force computed with filtered data is compared to the axial force reconstructed from axial acceleration by deconvolution in Figure 19. This figure demonstrates that there is higher frequency content in the reconstructed force by deconvolution than in the force computed from filtered acceleration data.

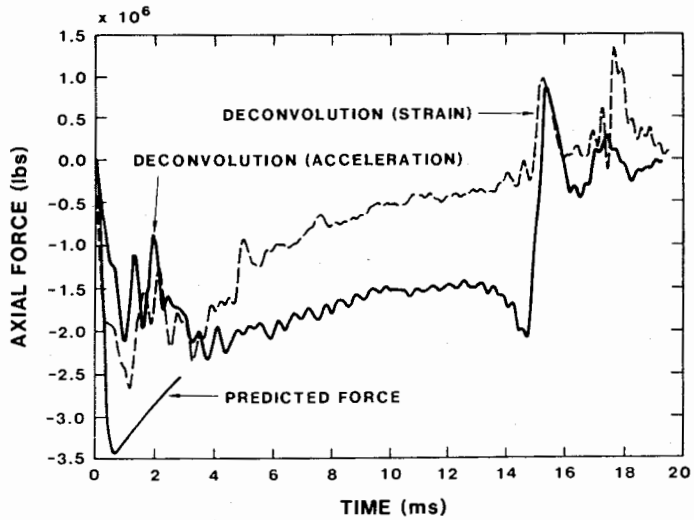

FIGURE 20: Comparison of Predicted Force Using GNOME with Reconstructed Forces by Deconvolution from Acceleration and Strain Data

variability in penetration parameters, typically 20-50%. Therefore, many tests at the same conditions are necessary to account for this variability and to provide a good comparison with the GNOME prediction. The force reconstructed from the acceleration measurement was integrated with an impulse-momentum relationship to calculate the maximum velocity; this velocity is 2134 fps which compares favorably with the measured velocity of 1940 fps. The force reconstructed from the strain measurement yields a much lower velocity of 1305 fps because it reflects the difference in nose and tail forces over most of the penetration event.

The lateral forces in Figures 15 and 17 are similar to each other as expected because they represent forces in the two lateral planes. The oscillatory behavior of the two force during the first 2 ms depicts the change in the force direction as first the nose and then the tail enters the penetration medium. These forces compare well in magnitude and time of occurrence with the predicted lateral forces from GNOME [14] in Figure 21 provided by Robert J. Kipp, Division 1522. However, the forces are different in character because the spatial characteristic of the strain gage provides a continuous force and the GNOME code calculates discrete forces.

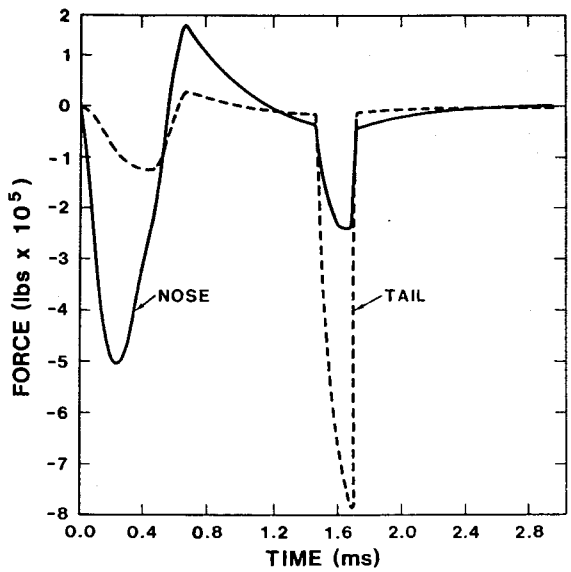

FIGURE 21: G-M118 Predicted Lateral Forces at the Nose and Tail Using GNOME

There are uncertainties in the reconstruction of penetration forces by the deconvolution technique presented here. There was considerable out-of-axis response observed in the the structural tests as shown in Figures 5-7. It is not known whether the out-of-axis response is entirely due to structural coupling or due partially to structural coupling and partially to a misalignment of the SEPW with the Reverse Hopkinson bar. More detailed measurements of the alignment of the Reverse Hopkinson bar test configuration as well as measurements of the modal properties of the SEPW for high-level force inputs would have to be made to determine the source of the out-of-axis response. Also, the boundary conditions for the structural tests were free-free which does not correspond to the penetration boundary conditions for the entire event. The change in the frequency response functions with the changing boundary conditions during penetration should be investigated to determine the effect on the force reconstruction process.

An implicit assumption in the force reconstruction conducted for the SEPW is that the reconstructed forces are acting at the same points that the forces were applied for the structural tests, that is at the nose. This assumption is valid for the forces during the first part of the penetration but becomes less credible at some point in the penetration event because the forces are distributed over the SEPW structure. More instrumentation locations are needed to resolve the distributed forces; the response measurements might then be analyzed by an estimation technique to yield a distributed force or by the Sum of Weighted Accelerations Technique, SWAT, [15] which can provide the force about the center of gravity as well as the applied moment [16].

14. N. T. Davie and M. A. Richgels, GNOME: An Earth Penetrator Code, SAND82-2358, (Albuquerque, NM: Sandia National Laboratories, May 1983).

15. T. G. Priddy, D. L. Gregory, and R. G. Coleman, "Strategic Placement of Accelerometers to Measure Forces by the Sum of Weighted Accelerations," SAND87-2567 (Albuquerque, NM: Sandia National Laboratories, January 1988).

16. T. G. Priddy, D. L. Gregory, and R. G. Coleman, "Measurement of Time-Dependent External Moments by the Sum of Weighted Accelerations," SAND88-3081 (Albuquerque, NM: Sandia National Laboratories, February 1989).

DISTRIBUTION:

1414	B. K. Christensen
1521	S. W. Attaway
1522	R. C. Reuter, Jr.
1522	R. J. Kipp
1522	D. R. Martinez
1524	A. K. Miller
5111	D. N. Bray
5111	W. J. Patterson
5111	L. B. Traylor
5115	S. D. Meyer
5115	K. R. Eklund
5115	R. K. Thomas
5121	D. F. McVey
5144	D. E. Ryerson
5144	R. J. Franco
5144	G. C. Hauser
5144	V. P. Salazar
5144	W. R. Wood
5160	G. R. Otey
5165	J. M. Freedman
5165	W. J. Errickson
5165	N. R. Hansen
5165	J. S. Ludwigsen
7290	T. S. Church
7522	O. M. Solomon, Jr.
7523	P. L. Walter
7540	T. B. Lane
7541	T. J. Baca
7541	F. A. Brown
7541	N. T. Davie
7542	T. G. Priddy
7542	V. I. Bateman (20)
7542	R. A. May
7543	R. Rodeman
7543	T. G. Carne
7543	J. P. Lauffer
7544	D. O. Smallwood
7544	D. L. Gregory
7544	T. L. Paez
7545	J. L. Mortley
7551	O. J. Burchett
8152	J. C. Swearengen
8171	C. T. Oien
8182	D. B. Nelson
8241	G. A. Benedetti
8316	J. Lipkin
8436	N. A. Lapetina
8462	R. I. Peterson
8462-1	D. C. Stoner
9122	R. H. Braasch
9122	M. J. Forrestal
9122	M. M. Hightower
9122	E. G. Kadlec
9122	T. M. Leonard
9122	R. C. Lundgren
9122	V. K. Luk
9122	W. K. Tucker
9122	C. W. Young
9122	E. W. Young
3141	S. A. Landenberger (5)
3151	W. I. Klein (3)
8524	J. A. Wackerly

Lawrence Livermore Laboratory (3)
Jose E. Hernandez, L-339
Henry S. Freynik, L-145
Engineering Measurement Section
P.O. Box 808
Livermore, CA 94550

Los Alamos National Laboratory (3)
Roger W. Taylor, WX-1, MS F634
Richard W. Macek, WX-11, MS C931
Donald L. Upham, WX-1, MS C936
P.O. Box 1663
Los Alamos, NM 87545

CTF-066468

Enclosure 1: #61

Unique Document # SA6200087840000 JAN 11 1985

RECEIVED

JAN 24 '91

CENTRAL TECH FILE

TEST NO.: HTW-1 R803414-1

TEST DATE: November 14, 1984

TEST SITE: Antelope Lake Concrete Target

Davis Gun Barrel Pressure, & Earth
Penetrator Accelerometer Data

HTW-1

Prepared by [signature] 7522

Approved by Pete C Hernandez 7522

Distribution:

5142	W. V. Hereford
5142	W. R. Wood
5146	C. W. Sprague (EG&G)
5146	A. F. Huters
5226	P. L. Walter
5341	C. E. Dalton
5341	C. W. Young
5341	M. M. Hightower (4)
5347	R. K. King
7173	L. W. Lathrop
7522	F. D. Gutierrez

CONFIRMED TO BE UNCLASSIFIED
AUTHORITY DOE/NN-52
BY R.H. SMILEY RHS, ADD
2-22-96
Nancy Connelly, ADD, 5010.23 7/8/05
HR Bennett, ADD, HS 93, 5/11/07

8784

28P

November 14, 1984

INSTRUMENTATION FOR PENETRATOR TEST HTW-1

A BSS system with 8 data inputs.

All data inputs were used for acceleration data.

Type of accelerometer: Endevco 2263 20k Potted in Adeprene L-100

High bit rate: 250K Bits/sec.

Memory load time: 192ms

Memory capacity: 49,152 Bits

Bits per Word: 6

Data Sample Rates:		
	Axial Acceleration	20,480 samples/sec.
	Lateral Acceleration	10,240 samples/sec.

FUNCTION	RANGE	ACCELEROMETER TYPE	ACCELEROMETER SERIAL NO.
Accel., in soil, long (X)	+5,000g -15,000g	Endevco 2263	AA21
Accel., in soil, lat. (Y)	±10,000g	Endevco 2263	AA21
Accel., in soil, lat. (Z)	±10,000g	Endevco 2263	AA21

This system contained characterized low pass filters on the accelerometer amplifiers providing the capability of data deconvolution if desired.

Data filter 6db point:		
	(X) Axial Data	3025Hz
	(Y) Lateral Data	3000Hz
	(Z) Lateral Data	3000Hz

This penetrator was fired into the Antelope Lake target at T.T.R. on November 14, 1984.

Launch velocity: 2116 ft./sec.

Angle of attack: 0°

Gun angle: 20° (from vertical)

Pressure instrumentation: Yes

R80341400

HTW-1 BARREL PRESSURE

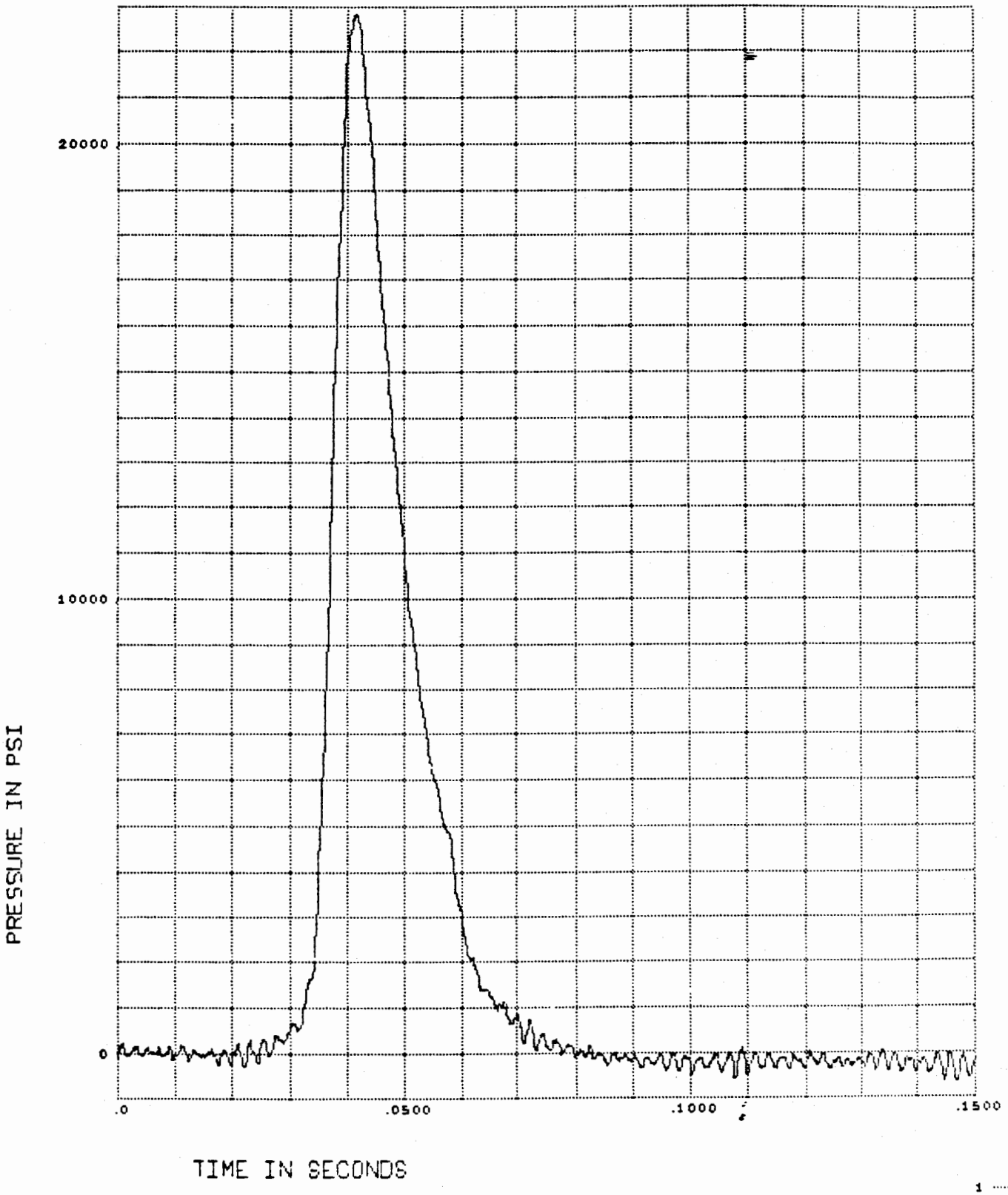

HTW-1

TEST DATE 11-14-84

TARGET DESCRIPTION

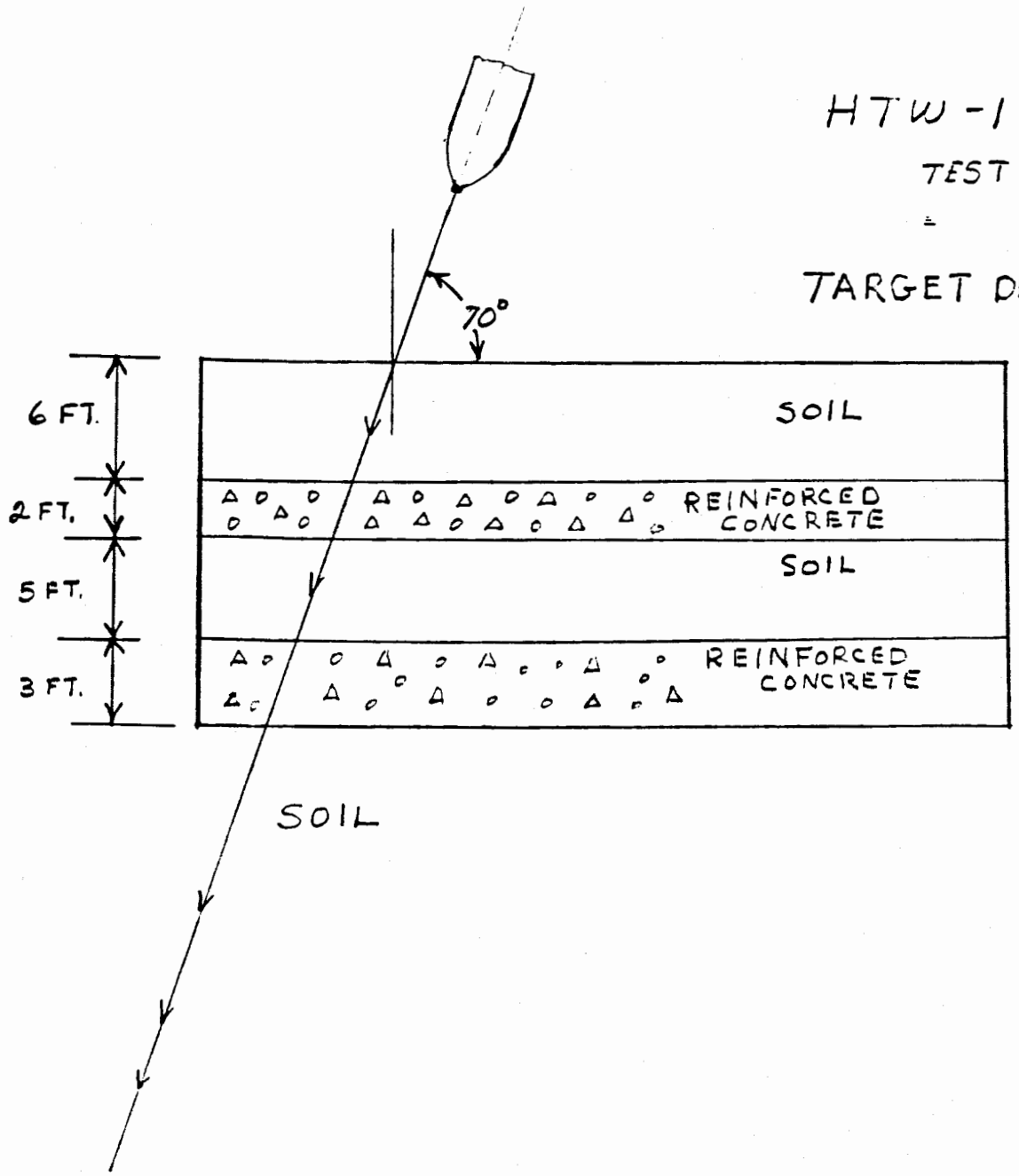

Wood 5142

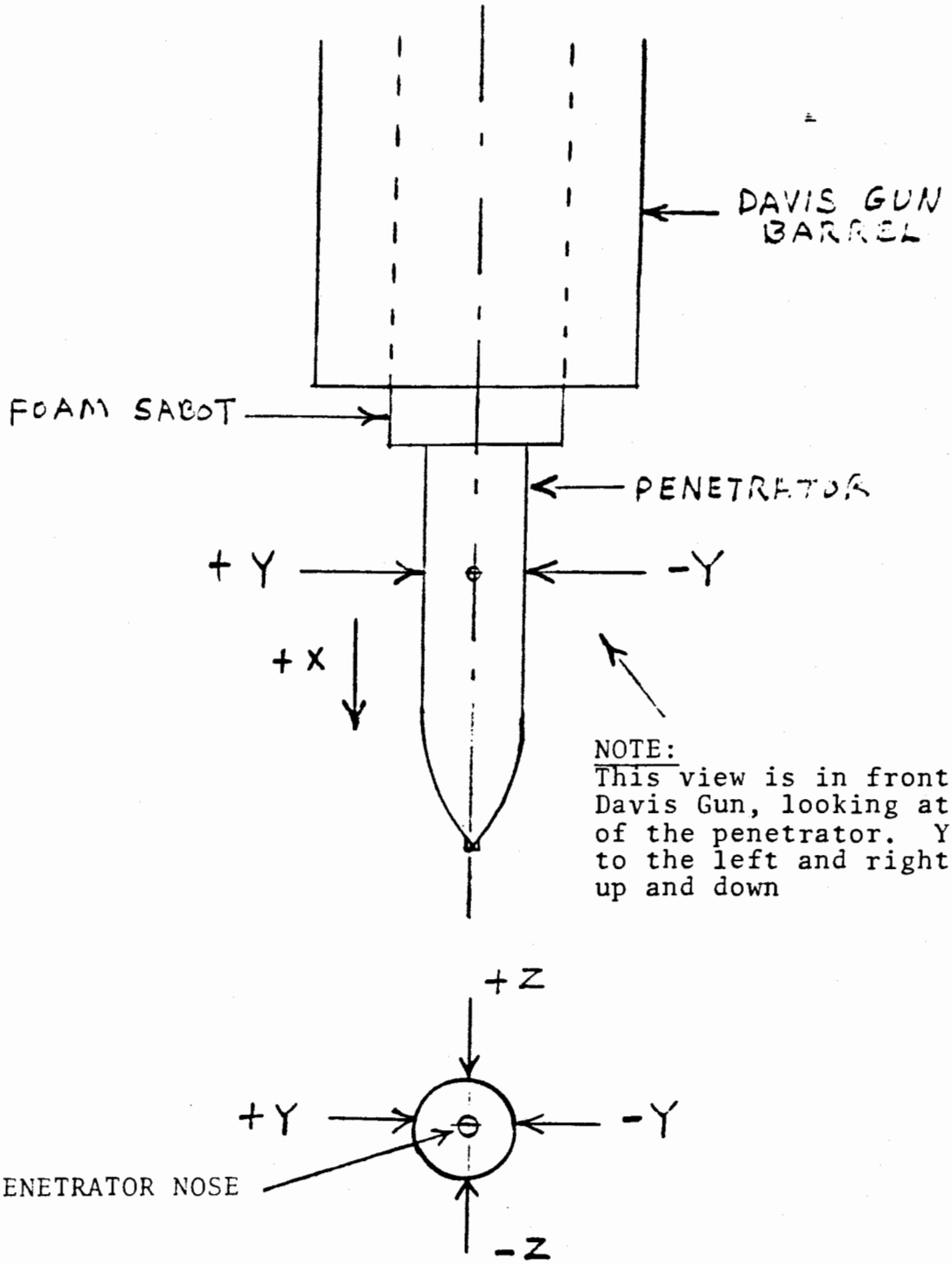

NOTE:
This view is in front of the Davis Gun, looking at the nose of the penetrator. Y Axis is to the left and right, Z is up and down

HTW-1
ACCELEROMETER
COORDINATE SYSTEM

R803414 HTW-01 X AXIS ACCELEROMETER

DAVIS GUN PENETROMETER TEST

A

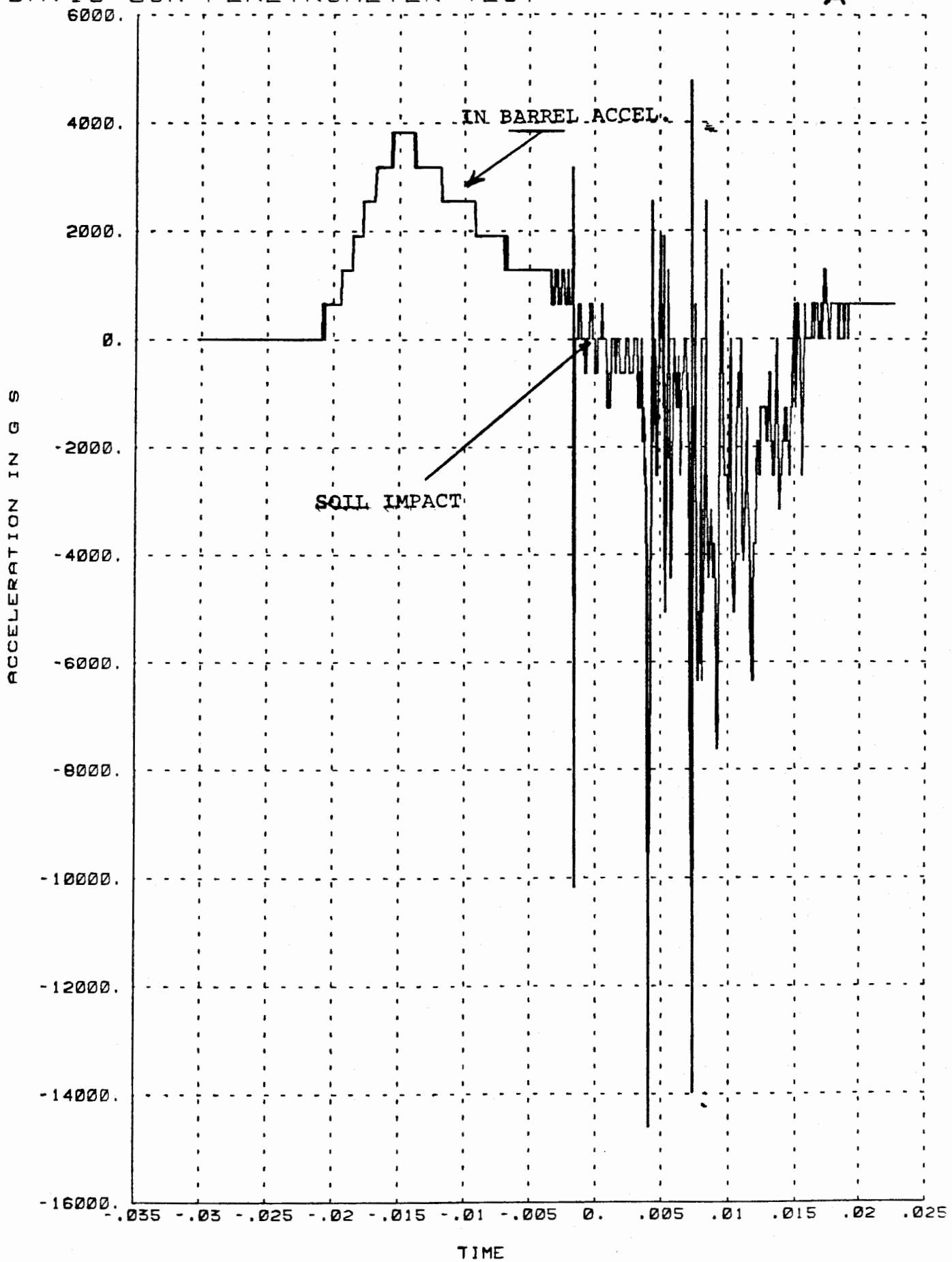

TIME IN SECONDS

R803414 HTW-01 X AXIS ACCELEROMETER

DAVIS GUN PENETROMETER TEST

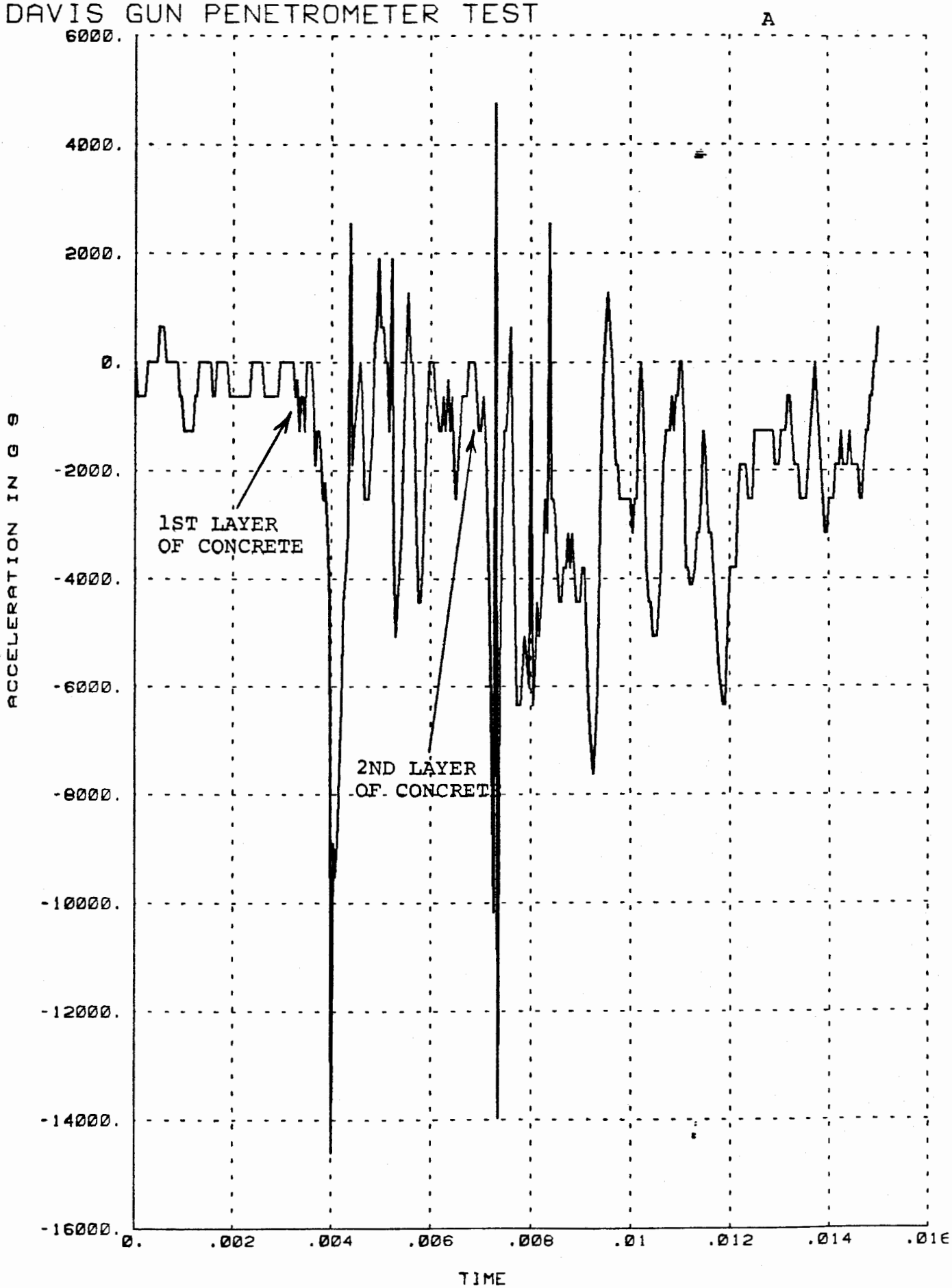

TIME IN SECONDS

R803414 HTW-01 X AXIS ACCELEROMETER

DAVIS GUN PENETROMETER TEST

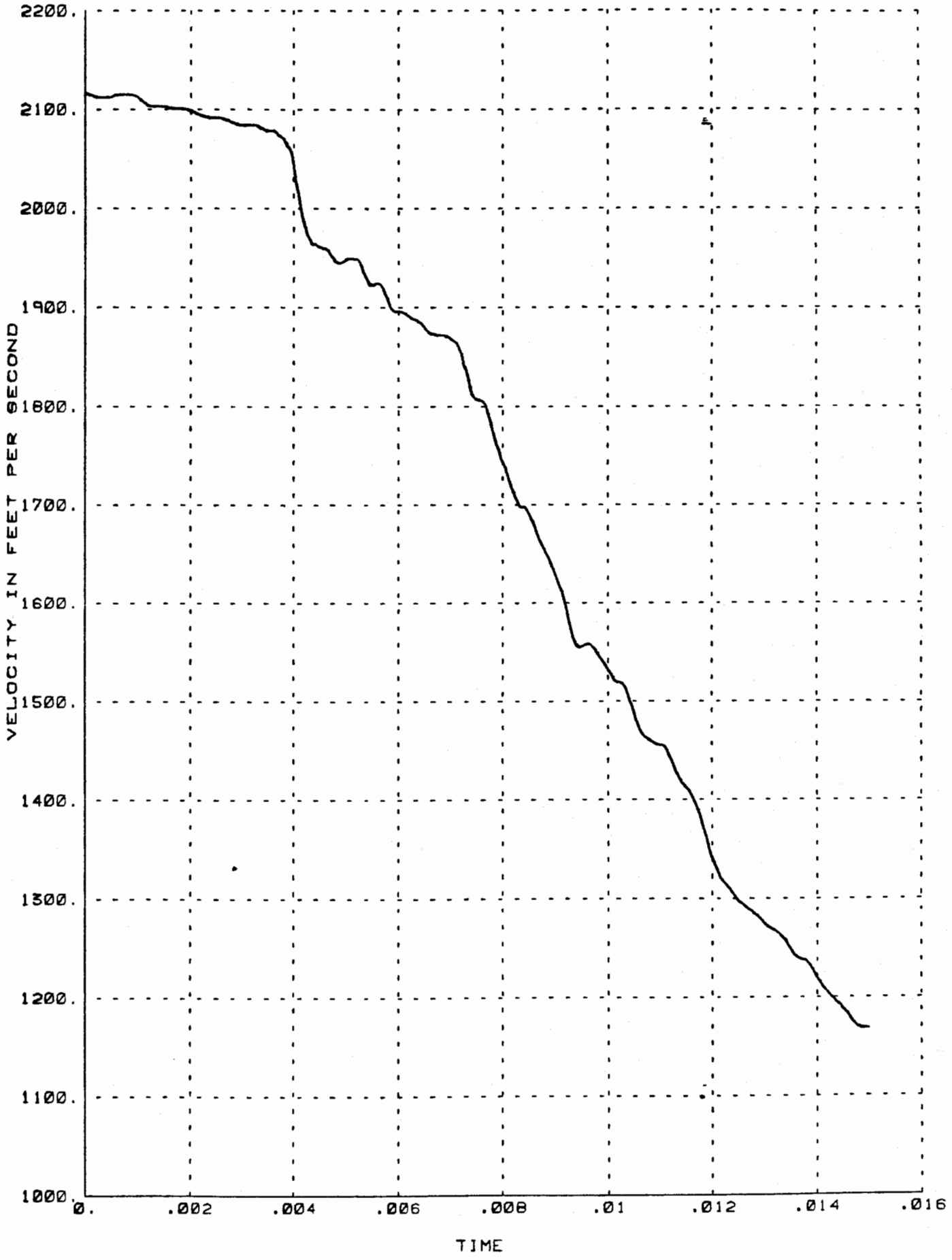

TIME IN SECONDS

R803414 HTW-01 X AXIS ACCELEROMETER

DAVIS GUN PENETROMETER TEST

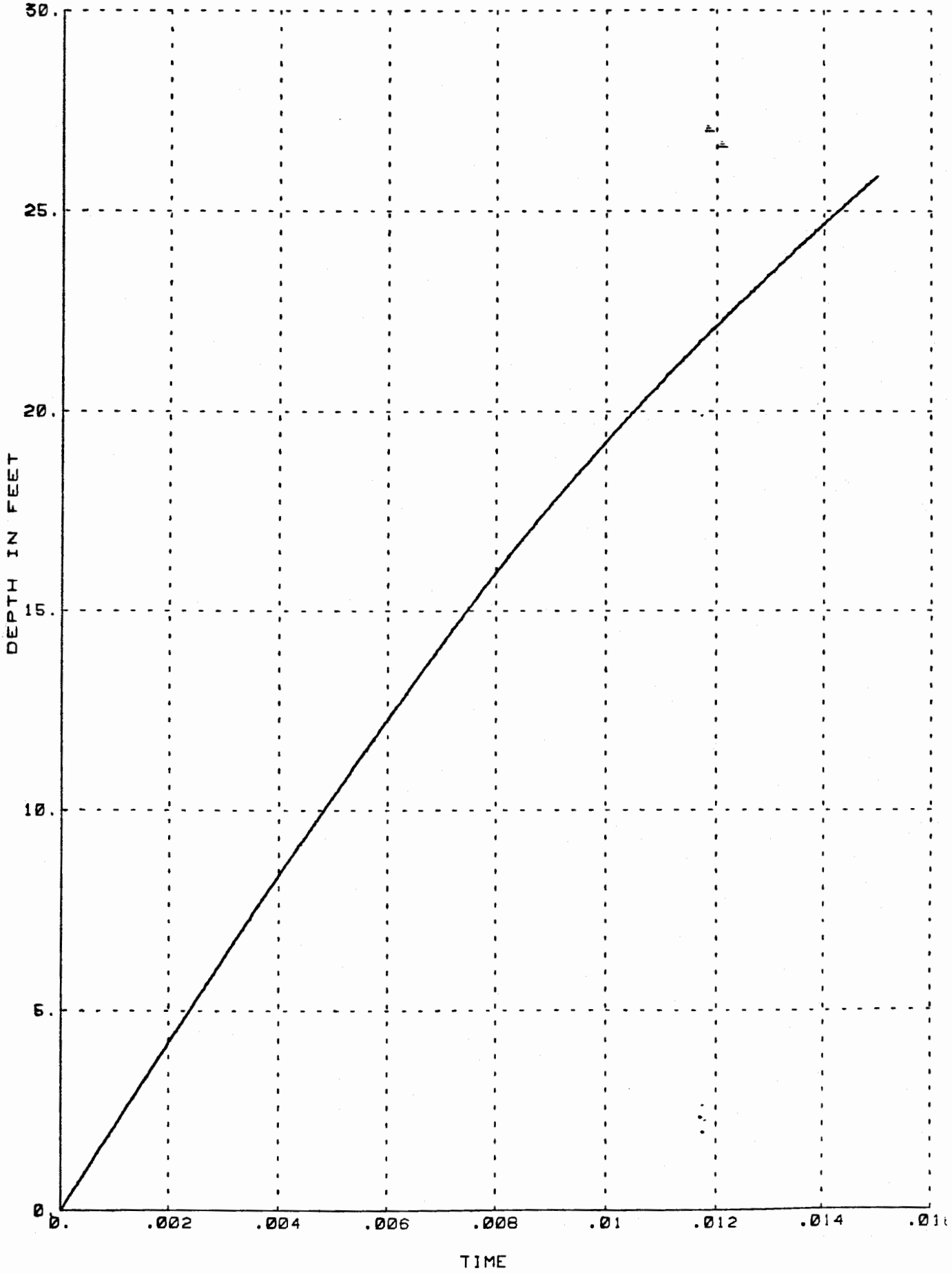

TIME IN SECONDS

R803414 HTW-01 VELOCITY VS DISPLACEMENT

DAVIS GUN PENETROMETER TEST

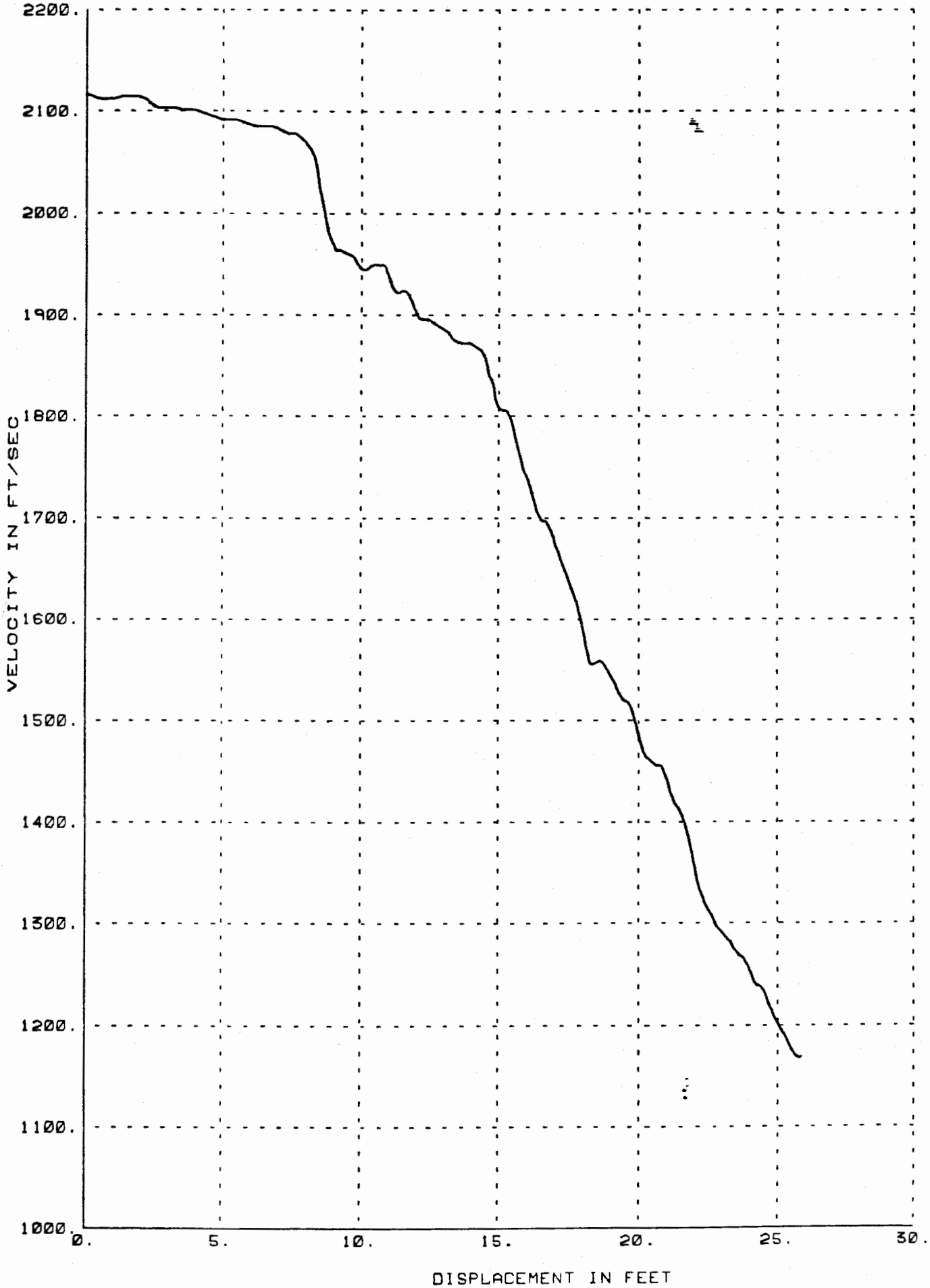

R803414 HTW-01 ACCELERATION VS DISPLACEMENT

DAVIS GUN PENETROMETER TEST

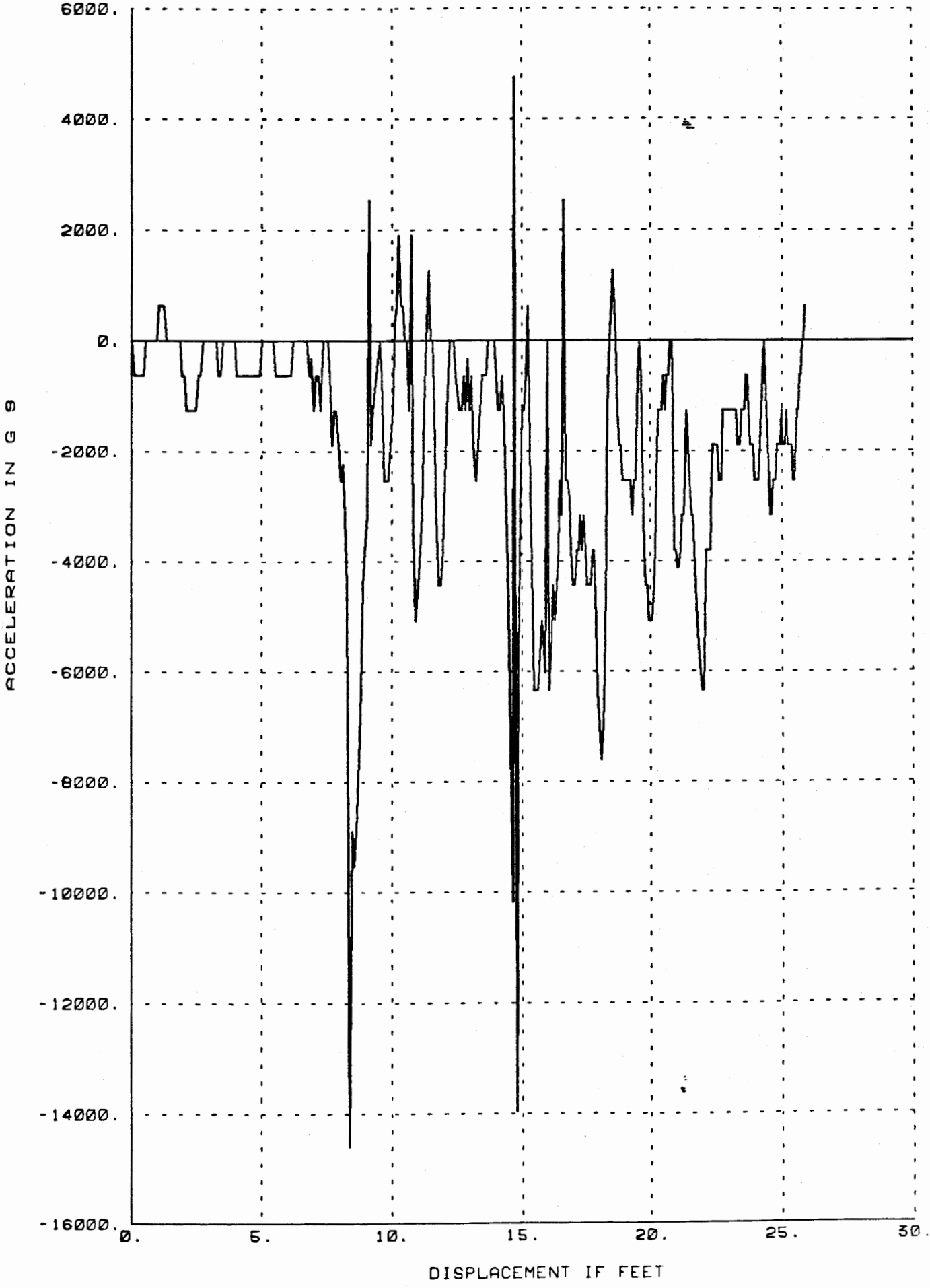

R803414 HTW-01 X AXIS ACCELEROMETER

DAVIS GUN PENETROMETER TEST 500HZ LPF

D

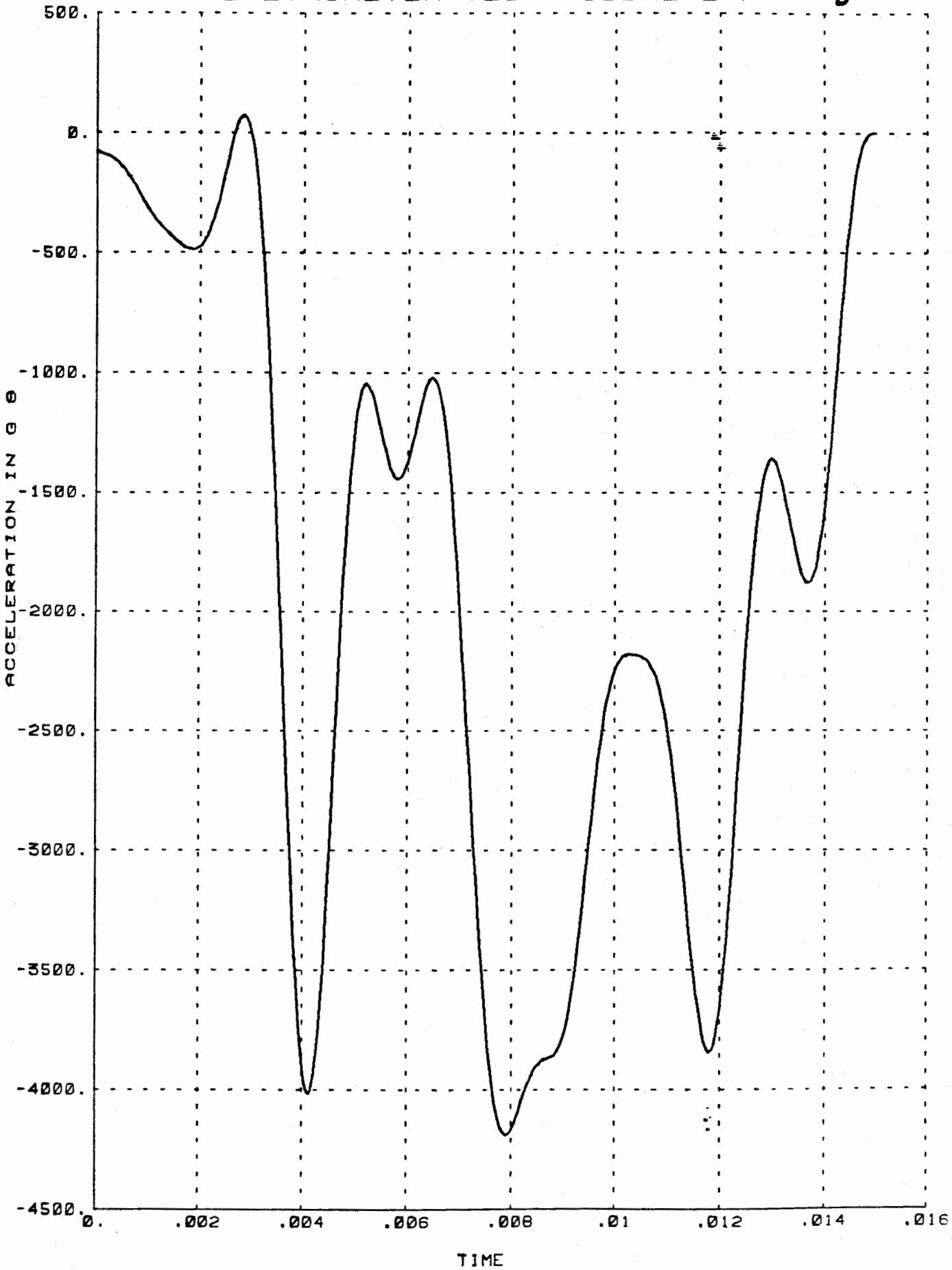

TIME IN SECONDS

R803414 HTW-01 X AXIS ACCELEROMETER

DAVIS GUN PENETROMETER TEST 200HZ LPF

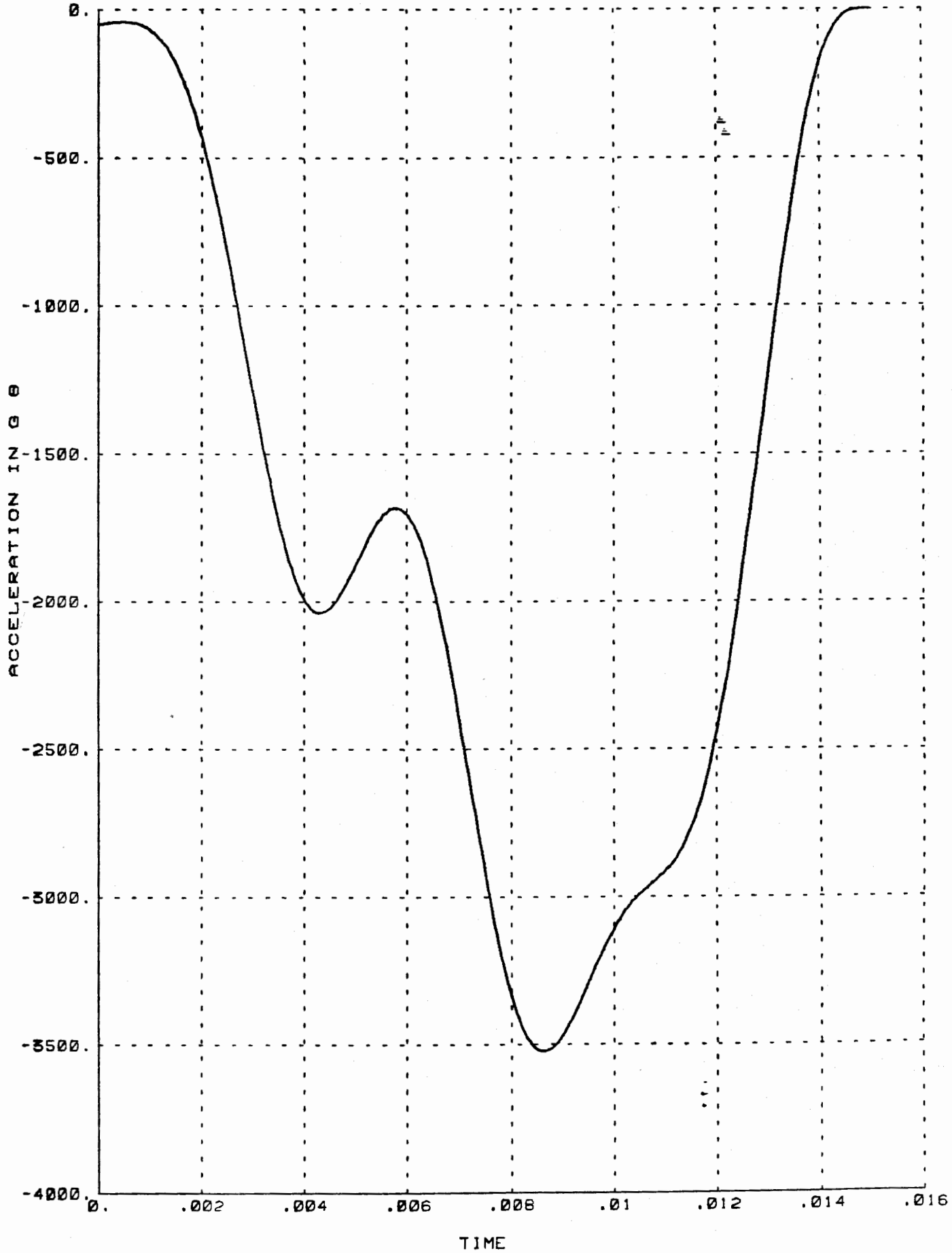

TIME IN SECONDS

R803414 HTW-01 Y AXIS ACCELEROMETER

DAVIS GUN PENETROMETER TEST 2K LPF

B

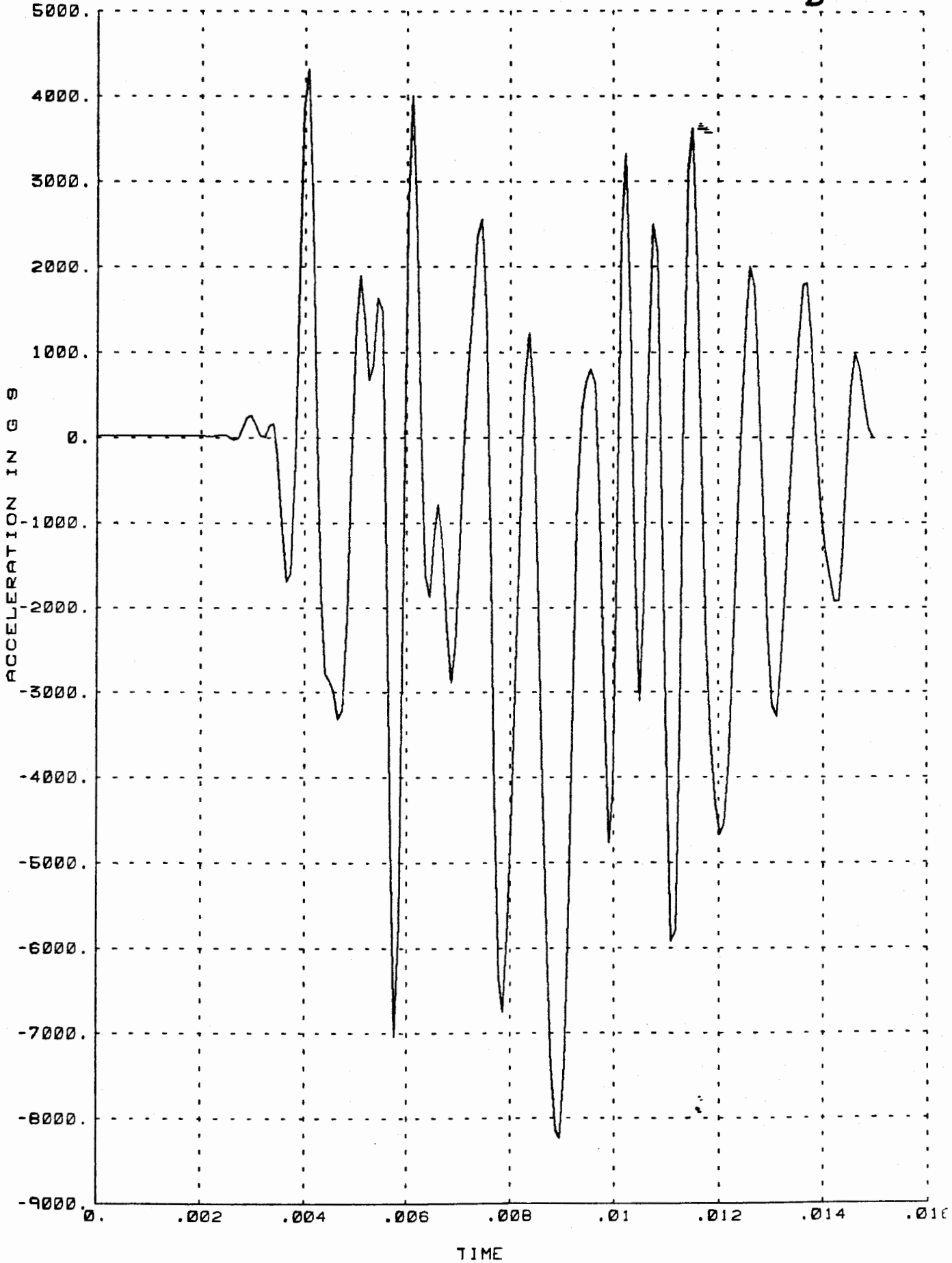

TIME IN SECONDS

R803414 HTW-01 Y AXIS ACCELEROMETER

DAVIS GUN PENETROMETER TEST 500 HZ LPF D

TIME IN SECONDS

R803414 HTW-01 Z AXIS ACCELEROMETER

DAVIS GUN PENETROMETER TEST

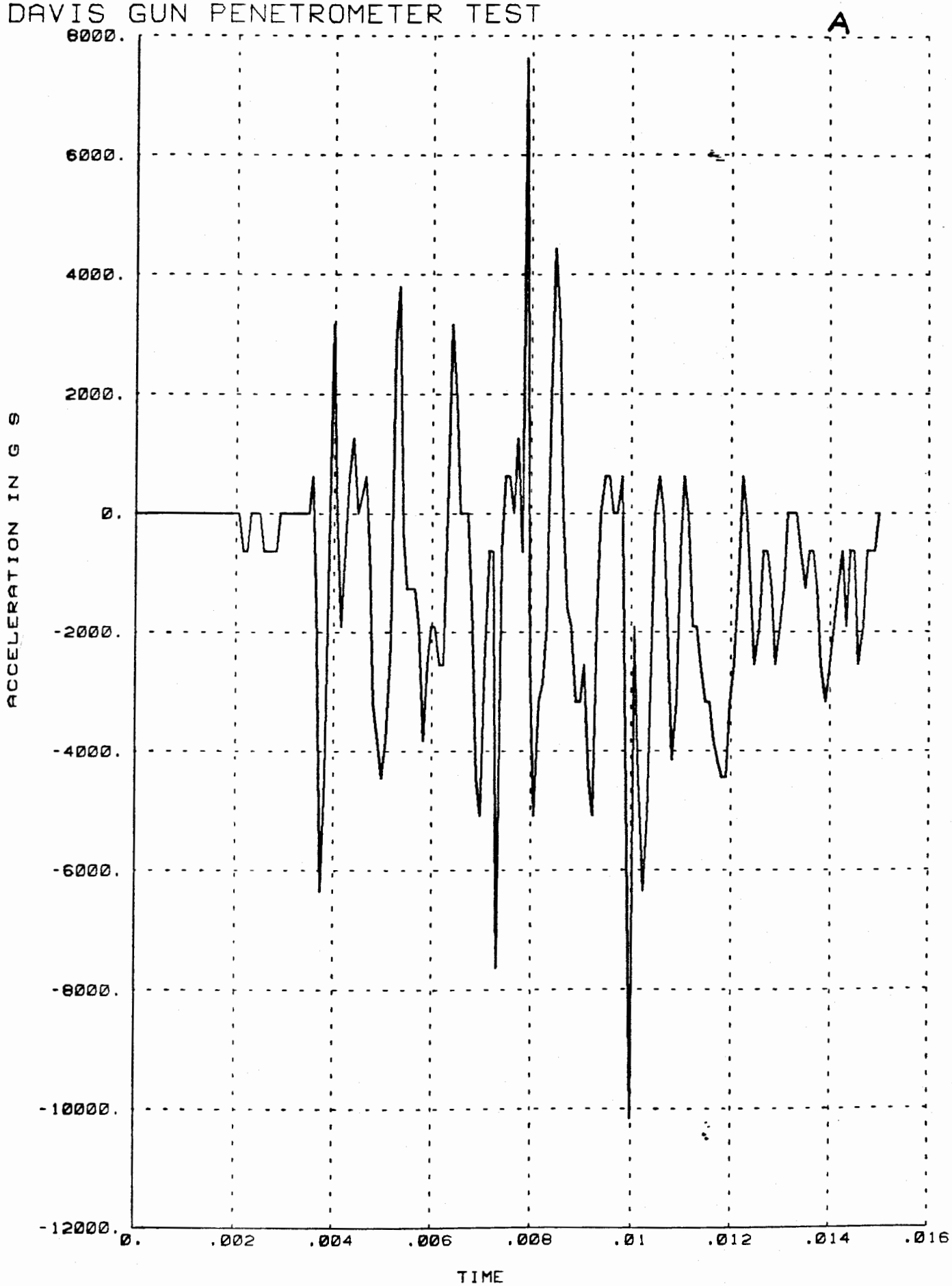

TIME IN SECONDS

R803414 HTW-01 Z AXIS ACCELEROMETER

DAVIS GUN PENETROMETER TEST 2K LPF

B

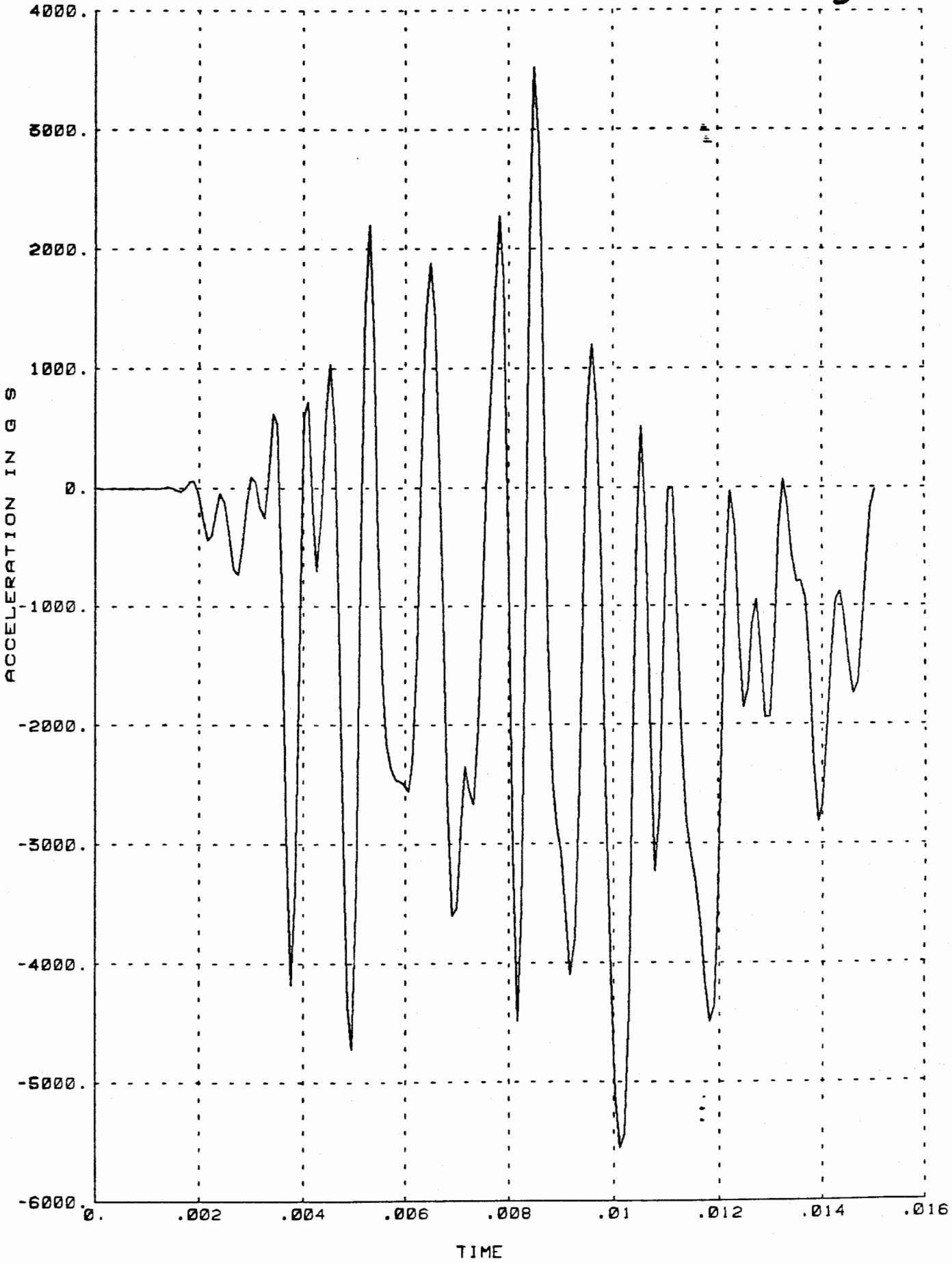

TIME IN SECONDS

R803414.HTW-01 Z AXIS ACCELEROMETER

DAVIS GUN PENETROMETER TEST 500 HZ LPF

D

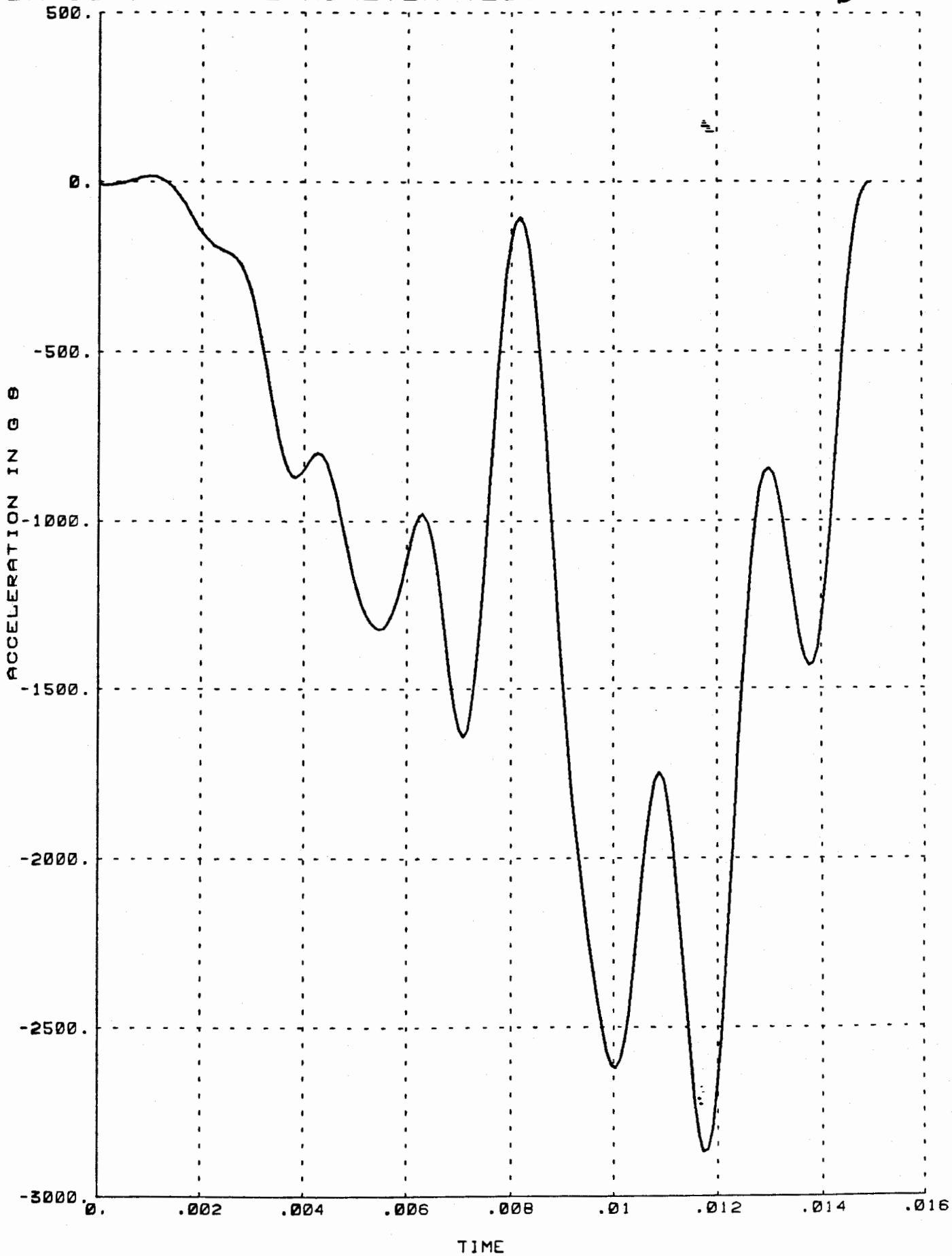

TIME IN SECONDS